Drug Design, Development and Therapy

Dovepress
Taylor & Francis Group

Open Access Full Text Article

ORIGINAL RESEARCH

Single vs Dual Lactose-Polyethylene Glycol 3000 Microcarrier Systems for Pulmonary Salmeterol and Fluticasone Targeted Delivery

Muhammad Waseem Akram[1,2], Badrul Hisyam Zainudin[3], Mohamed Effendi Mohamed Tenang[4], Tin Wui Wong[1,2,5]

[1]Non-Destructive Biomedical and Pharmaceutical Research Centre, Smart Manufacturing Research Institute, Universiti Teknologi MARA Selangor, Puncak Alam, 42300, Malaysia; [2]Particle Design Research Group, Faculty of Pharmacy, Universiti Teknologi MARA Selangor, Puncak Alam, 42300, Malaysia; [3]Malaysian Cocoa Board, Cocoa Innovation and Technology Centre, Nilai, Negeri Sembilan, 71800, Malaysia; [4]Tenang Pharma Sdn Bhd, Nilai, Negeri Sembilan, 71800, Malaysia; [5]Department of Industrial Pharmacy, Faculty of Pharmacy, Silpakorn University, Nakhon Pathom, 73000, Thailand

Correspondence: Tin Wui Wong, Non-Destructive Biomedical and Pharmaceutical Research Centre, Smart Manufacturing Research Institute, Universiti Teknologi MARA Selangor, Puncak Alam, 42300, Malaysia, Email wongtinwui@uitm.edu.my

Background: Agglomeration/microparticulation of anti-asthmatic/anti-inflammatory salmeterol (SX) and fluticasone (FP) in a single vehicle rendered inefficient pulmonary drug redispersion and site targeting. This study designed externally drug coated dual-microcarrier against single microcarrier (SX external coat/FP internal coat) systems and examined their pulmonary drug delivery/targeting profiles.

Methods: Spray-dried lactose-polyethylene glycol 3000 microcarriers were prepared with magnesium stearate lubricant added where applicable. Both single- and dual-microcarrier systems were subjected to cascade impactor analysis against microcarrier particle size and formulation attributes. In vivo pharmacokinetics/pharmacodynamics profiles were assessed.

Results: Small microcarrier (~5 μm) was preferred over larger ones for SX targeting at primary to terminal bronchi. Magnesium stearate promoted drug inhalation via reducing microcarrier aggregation and keeping it small for drug deposition and inhalation. Drug-coated single- and dual-microcarrier systems enabled SX release at upper lung and FP release at lower lung. Drug-coated dual-microcarrier enhanced FP inhaled deposition at lower lung due to the absence of external SX barrier and opportunistic hydrophobic aggregation of SX with magnesium stearate-FP deposited on the same microcarrier. Dual-microcarrier increased pulmonary drug retention with a marginal rise in systemic drug levels and reduced inflammatory lymphocytes/eosinophils/neutrophils infiltration, IL-4/5/9/13 release, mucus production, and bronchoconstriction.

Conclusion: Dual-microcarrier is more efficient than single-microcarrier in pulmonary SX/FP delivery.

Keywords: asthma, aerosolization, dual-microcarrier, inhalation, single-microcarrier

Introduction

Asthma, the most common chronic immunological disease of airways, affects approximately 300 million people worldwide and is projected to exceed 400 million by 2025.[1] Airway inflammation, smooth muscle constriction, and mucus hypersecretion are hallmark symptoms in asthmatic patients. T-helper type 2 (Th2) asthma, also known as allergic asthma, is relatively common and is associated with the expression of interleukin (IL)-4, IL-5, IL-9, IL-13, and immunoglobulin E (IgE).[2,3] According to the global initiative for asthma guidelines, the combination therapy of inhaled corticosteroids (eg fluticasone propionate) and long-acting beta agonists (eg salmeterol xinafoate) is the mainstay therapy for persistent asthma and chronic obstructive pulmonary disorder management.[4]

Salmeterol xinafoate (SX; molecular weight = 603.7 g/mol) targets β2-adrenoceptor located on smooth muscles of the upper respiratory tract to relieve asthma via bronchodilation.[5,6] SX possesses a long hydrophobic tail which promotes its binding to receptor for more than 12 hours. A randomized controlled clinical trial highlighted that delivery of

https://doi.org/10.2147/DDDT.S582476
Received: 3 December 2025
Accepted: 16 February 2026
Published: 26 February 2026

Graphical Abstract

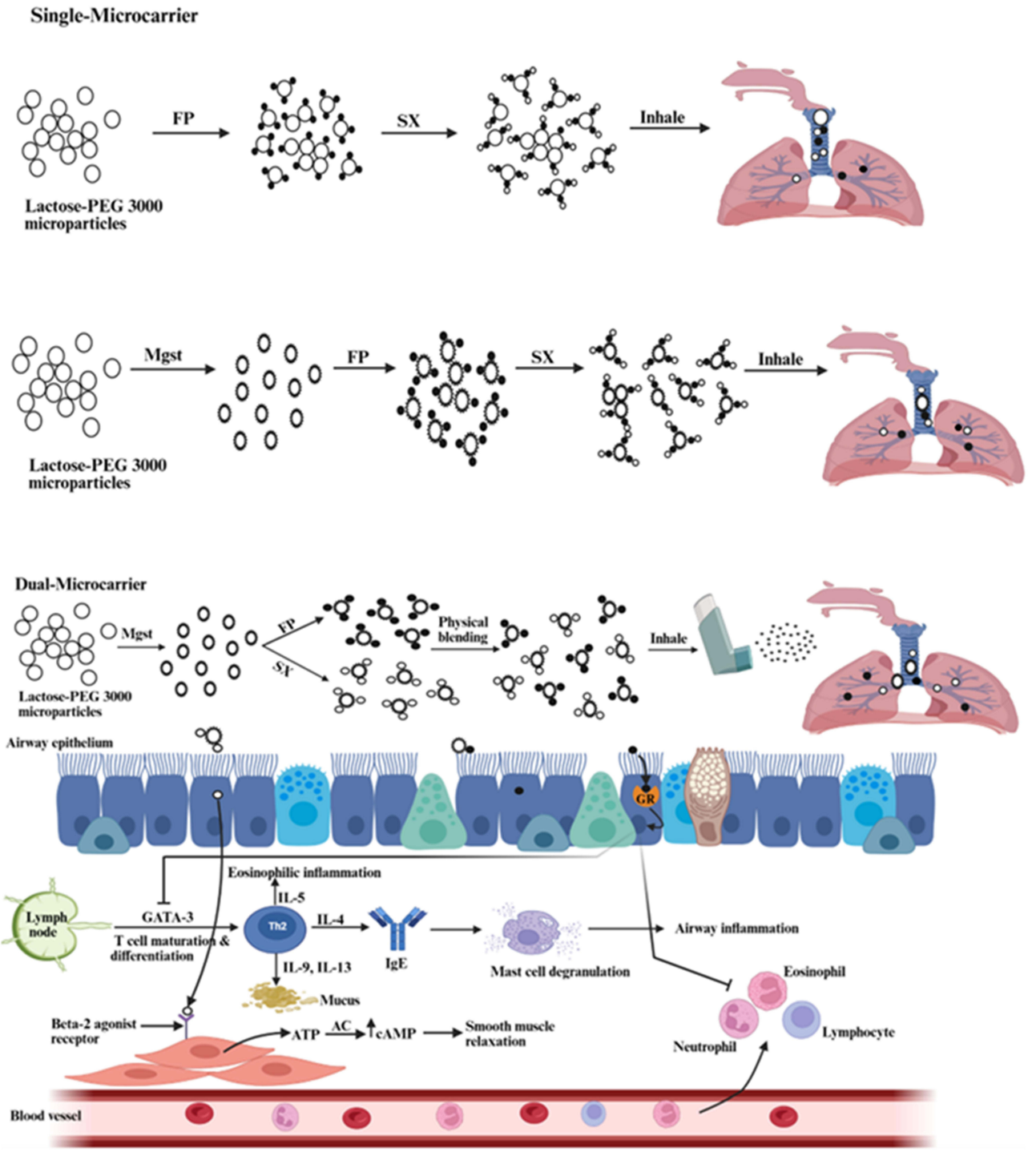

SX: salmeterol xinafoate; FP: fluticasone propionate; Mgst: magnesium stearate

a β2-agonist to the upper airway produced a more profound bronchodilation compared with delivery to the distal region of lungs.[7] Fluticasone propionate (FP; molecular weight = 500.6 g/mol) is a trifluorinated androstane drug conjugated with propionic acid.[8] Its highly lipophilic character enhances its ability to integrate into lung membranes resulting in

prolonged residence. With reference to chronic obstructive pulmonary disorder, FP exerts anti-inflammatory effects by acting on cytoplasmic glucocorticoid receptor present in the epithelial cells of the lower lungs. These complexes translocate to the nucleus to impede the inflammatory cascade by switching off GATA-3 that controls the Th2 cytokine expression.[9]

The lungs serve as an appealing target for the delivery of drugs intended for pulmonary disease treatment.[10] Pulmonary drug delivery offers several advantages, including high bioavailability, evasion of first-pass hepatic metabolism, and protection from harsh gastrointestinal pH environment and enzymatic degradation. Despite these merits, the innate defense mechanism of the respiratory tract not only restricts the pathogens entry but also traps the inhaled drug particles within the complex anatomical structure, hence limiting particle deposition mainly to the upper respiratory tract.[11] To ensure drug deposition in the lower lung, the inhaled particles should ideally have an aerodynamic diameter between 1 μm and 5 μm.[12]

SX and FP have been formulated in the form of an inhalable drug powder for asthma treatment. The common approach involves aggregating both drugs into a single system of 1 to 3 μm for pulmonary inhalation.[5,8,13–16] To date, most inhaled dry powders are formulated as agglomerates, microencapsulated particles, and composite microparticles.[17] These dosage forms are associated with several limitations such as restricted particle deposition to the upper respiratory tract, risks of low drug particle redispersion in the lung, and inconsistent or inadequate drug release behaviour.[12] Directly blending of drug particles onto a carrier has been advocated as the formulation approach that could overcome these hurdles.[12,18] The drug particles are not bound by binders directly into a microstructure, allowing aerosolization and inhalation to proceed without interference by these excipients. Dry powder inhalers are anticipated to enable targeted delivery of different drugs to both upper and lower respiratory tracts in a single administration through formulation strategies (multiple drug coat to initiate sequential release) and carrier particle size modulation (mix of large and small particles to target at upper and lower lung regions respectively), although such potential has yet to be investigated experimentally and verified in the clinical practice. On this note, this study aims to design single- vs dual-microcarrier systems for targeted delivery of SX and FP via direct physical blending of drug particles with lactose-polyethylene glycol (PEG) 3000 microparticles acting as the drug carrier. Lactose-PEG 3000 microparticles are selected as the carrier of choice as they exhibit a stable physicochemical stability.[12] The single-microcarrier system is developed by first depositing FP adjacent to the surfaces of lactose-PEG 3000 microparticles (interior layer) followed by SX as the exterior layer in contact with the immediate lung environment. Aerosolization and inhalation of this physical blend are envisaged to result in SX release at the upper lung followed by FP dispersion at the lower lung. The dual-microcarrier system involves depositing SX and FP onto lactose-PEG 3000 microparticles of different particle sizes followed by physical blending of both. The larger lactose-PEG 3000 microparticles are envisaged to deposit SX at the upper lung whereas smaller lactose-PEG 3000 microparticles deliver FP to the lower lung. Individual drug deposition reduces the dispersion barrier of FP caused by the external SX layer in the single-microcarrier system.

Materials and Methods

Materials

SX and FP (Aarti Industries Limited, India) were used as the submicron drugs of interest for asthma treatment. Lactose monohydrate (Sorbolac 400, Meggle, Germany) was utilized as the matrix material of microparticles with PEG 3000 (Merck, Germany) as the stabilizer to reduce lactose hygroscopicity and ethanol (Absolute; Merck, Germany) as the surfactant to reduce the spray-dried particle size of lactose. Magnesium stearate (R & M chemicals, UK) was used as the lubricant of solid lactose particles. Methanol and acetonitrile (HPLC grade; Merck, Germany) were employed in the analytical quantification of SX and FP. Ovalbumin (OVA, lyophilized powder grade V: ≥98% purity (agarose gel electrophoresis); Sigma Aldrich, USA) was utilized as an allergenic inducer for the development of an asthmatic animal model. Aluminum hydroxide (Thermo Scientific, USA) served as an adjuvant to enhance the ovalbumin action.

Preparation of Lactose-PEG 3000 Microparticles

Lactose-PEG 3000 microparticles (F1-F9) were prepared using the spray drying technique (TwinNanoSpray, UiTM, Malaysia) with varying concentrations of lactose and PEG 3000, and ethanol introduced to the mixture of lactose and PEG 3000 where applicable. An accurately weighed amount of lactose was first dissolved in distilled water, followed by the addition of PEG 3000 and/or ethanol with amount expressed relative to the lactose mass, at 25 ± 1°C under continuous magnetic stirring (Table 1). The feed solution was spray-dried (nozzle diameter = 0.4 mm) using the processing parameters given in Table 1. The spray-dried powder was harvested using a rubber spatula from the collecting electrode, transferred to a vial and conditioned in a silica gel desiccator for at least 5 days. The powder was then sieved using a 50-mesh sieve prior to physicochemical characterization.

Physicochemical Characterization of Lactose-PEG 3000 Microparticles

Size and Specific Surface Area

The specific surface area, volume weighted median diameter (d_{10}, d_{50} and d_{90}), volume weighted mean diameter $D_{[4,3]}$, surface area weighted mean diameter $D_{[3,2]}$ and span of the lactose-PEG 3000 microparticles were determined using a laser diffraction particle size analyzer (Mastersizer 2000, Malvern Instruments Limited, UK), assisted by a dry powder dispersing system. Each sample was tested in triplicates and the results were averaged.

Morphology

The morphology of the lactose-PEG 3000 microparticles was characterized by scanning electron microscopy technique (SEM; Quanta 450 FEG, FEI, The Netherlands). The microparticles were first mounted on a carbon tape followed by sputter-coating with platinum using an automatic fine coater (JFC-1600 Auto Fine Coater, JEOL, Japan). The images were captured at 5000× magnification under an accelerating voltage of 5 kV. Representative images were captured for each sample. ImageJ software (NiH, USA) was utilized to measure the circularity (Circ) and surface roughness (Ra) of the microparticles from these images. Mean and standard deviation of Circ and Ra were calculated from nine measurements of three images.

Crystallinity

X-ray powder diffractometer (XRPD; Ultima IV, Rigaku Cooperation, Japan) was used to analyze the crystallinity of lactose-PEG 3000 microparticles. The sample was scanned at 5°/min over diffraction angles (2θ) of 5° to 30° using Cu-Kα (40 kV and 30 mA) as the X-ray resource. The crystallinity was calculated using the following equation:

$$\text{Crystallinity } (\%) = (I_{110} - I_{amor}) \times 100/I_{110} \quad (1)$$

where I_{110} = maximum diffraction intensity value at 20° and I_{amor} = intensity of amorphous diffraction at 16°. Triplicates were performed for each sample and the results were averaged.

Physicochemical Characterization of Drugs

Where applicable, the size, surface morphology and crystallinity of SX and FP were determined using laser diffraction particle size analyzer, SEM and XRPD techniques as outlined in the lactose-PEG 3000 microparticle characterization. The zeta potential profiles of SX and FP were determined using Zetasizer (Nano ZS 90, Malvern Instruments Ltd, UK) at 25°C. One mg of drug was briefly dispersed in 10 mL of deionized water using vortex mixer. The dispersion was filled into a capillary zeta cell for analysis. Triplicates were conducted for each drug and the results were averaged.

Density and Flow Property

A 5-mL measuring cylinder was used to determine the bulk and tapped densities of lactose-PEG 3000 microparticles, the drugs or their mixtures. The cylinder was first filled with a known quantity of powder, and the bulk volume was recorded. The quotient of powder weight to bulk volume is expressed as bulk density (ρ_b). The powder-filled cylinder was then tapped from a height of 4 cm onto a flat surface at 60 taps/min until no further reduction in volume was observed (after 180 taps). The tapped volume was recorded. The quotient of powder weight to tapped volume is known as tapped density (ρ_t). Carr's index and Hausner ratio were derived from the ρ_b and ρ_t values using the following equations:

Table 1 Formulation and Processing Parameters of Lactose-PEG 3000 Microparticles and Their Size and Specific Surface Area Attributes

Parameter	F1	F2	F3	F4	F5	F6	F7	F8	F9
	Formulation and processing								
Lactose monohydrate (%w/w)	2	2	2	2	1	1	1	1	2
PEG 3000 (%w/w)	2.5	2.5	1.25	0.625	1.25	0.625	0.625	0.625	1.25
Ethanol (%)	–	–	–	–	–	5	20	30	–
Inlet temperature (°C)	70	80	70	70	70	70	70	70	70
Outlet temperature (°C)	48	30	41.5	45	44	43	40	41	40.5
Feeding rate (mL/min)	2.2	2.2	1.3	1.3	1.3	1.3	1.3	1.3	3.0
Atomization ambient air pressure (bar)	5.5	5.5	5.5	5.5	5.5	5.5	5.5	5.5	5.5
Air flow rate (m/s)	2–2.5	2–2.5	2–2.5	2–2.5	2–2.5	2–2.5	2–2.5	2–2.5	2–2.5
Feeding tube	1	1	1	1	1	1	1	1	1
Size and specific surface area									
d_{10} (μm)	1.84 ± 0.01	3.80 ± 0.04	1.81 ± 0.01	2.30 ± 0.02	1.49 ± 0.02	2.86 ± 0.07	2.28 ± 0.51	1.48 ± 0.43	2.05 ± 0.03
d_{50} (μm)	7.89 ± 0.01	48.25 ± 1.43	5.87 ± 0.03	9.68 ± 1.01	9.66 ± 0.72	11.49 ± 0.29	10.54 ± 0.42	5.20 ± 0.41	9.71 ± 0.04
d_{90} (μm)	46.66 ± 0.67	171.43 ± 14.41	17.45 ± 1.10	46.60 ± 3.10	30.28 ± 0.54	35.94 ± 0.68	30.43 ± 4.71	13.39 ± 0.24	28.23 ± 1.92
$D_{[3,2]}$ (μm)	4.49 ± 0.00	9.81 ± 0.02	3.82 ± 0.01	5.71 ± 0.17	4.21 ± 0.31	6.08 ± 0.21	5.83 ± 0.45	3.28 ± 0.11	4.91 ± 0.35
$D_{[4,3]}$ (μm)	19.83 ± 0.95	61.05 ± 5.20	12.14 ± 2.15	19.61 ± 1.32	13.32 ± 0.37	17.04 ± 2.94	16.94 ± 5.44	6.80 ± 2.23	12.95 ± 0.86
Span	5.68 ± 0.07	3.15 ± 0.20	2.65 ± 0.08	4.06 ± 0.10	2.98 ± 0.11	2.87 ± 0.02	2.34 ± 0.28	2.61 ±0.40	2.89 ± 0.04
Specific surface area (m^2/g)	1.33 ± 0.01	0.60 ± 0.00	1.83 ± 0.04	1.21 ± 0.02	1.37 ± 0.04	0.95 ± 0.03	1.03 ± 0.07	1.63 ± 0.03	1.21 ± 0.02

https://doi.org/10.2147/DDDT.S582476

$$\text{Carr's index}(\%) = (1 - (\rho_b/\rho_t)) \times 100\% \quad (2)$$

$$\text{Hausner ratio} = \rho_t/\rho_b \quad (3)$$

Higher values of Carr's index and Hausner ratio denote a poorer powder flow. At least triplicates were conducted for each sample and the results were averaged.

In vitro Aerosolization and Inhalation

The aerosolization and inhalation profiles of the physical blend of drugs and lactose-PEG 3000 microparticles as well as the neat drugs were examined using an Andersen cascade impactor (ACI; Copley Scientific Ltd, UK). The cascade impactor was assembled from stage 0 to stage F, with all stages being clamped tightly using the FDA-approved silicon rubber to prevent any particle leakage during test. A glass fiber filter was placed under stage 7 to trap small leaking particles. To simulate the human respiratory tract, a pre-separator was connected with stage 0 and further linked with an induction port and a mouthpiece adapter. The ACI was attached with a critical flow controller and a vacuum source to perform the inhalation operation.

The cascade impactor analysis was conducted in multiple phases. In the first phase, the aerosolization and inhalation profiles of neat SX (200 μg) and FP (1000 μg) were analyzed in the absence of lactose-PEG 3000 microparticles. In the second phase, F3 and F9 were mixed with SX in a weight ratio of 9:1 keeping the SX content at 200 μg and subjected to cascade impactor analysis to identify inhalable lactose-PEG 3000 microparticles. In the third phase, specific amounts of inhalable lactose-PEG 3000 microparticles (10 mg, 20 mg, 40 mg and 80 mg) were gently mixed with FP (1000 μg) for 10 min followed by the addition of SX (200 μg) to the powder blend with gentle mixing for an additional 10 min before cascade impactor analysis. Both FP and SX, being near submicron in size, would be deposited onto the lactose-PEG 3000 microparticles. The SX was formulated as the outer most layer as it was designed to detach first and deposit in upper respiratory tract to relieve smooth muscle contraction and asthma. The inner FP would be released subsequently as particles travelled to the lower lungs to treat the inflammatory chronic obstructive pulmonary disease. In the fourth phase, different contents of magnesium stearate (2.5%, 5% and 10%), relative to the optimized weight of lactose-PEG 3000 microparticles (20 mg) determined in the third phase, were added to the lactose-PEG 3000 microparticles followed by FP (1000 μg) and then SX (200 μg). Magnesium stearate acted as a lubricant to reduce the aggregative behaviour of lactose-PEG 3000 microparticles. This increased the availability of smaller lactose-PEG 3000 microparticles for drug deposition and promoted the formation of overall smaller microparticulates efficient for inhalation. The aerosolization and inhalation profiles of SX (200 μg) and FP (1000 μg), using magnesium stearate (20 mg) as the sole carrier, were also compared with those of the lactose-PEG 3000 microparticles. In the fifth phase, both SX (200 μg) and FP (1000 μg) were introduced individually as the single drug layers onto the lactose-PEG 3000 microparticles (10 mg/drug) pre-blended with 5% magnesium stearate. The lactose-PEG 3000 microparticles/magnesium stearate/SX and lactose-PEG 3000 microparticles/magnesium stearate/FP were then physically mixed before cascade impactor analysis. The use of single drug layer was intended to eliminate the drug release barrier to the internal FP observed in the Phase 4 formulation.

The powder sample was prepared by blending lactose-PEG 3000 microparticles, magnesium stearate, SX and FP in the required quantity and sequence using a Falcon tube. Where applicable, the mixture was subjected to vortex stirring (Velp®, Scientifica, Italy) at 10 Hz for 5 min after each material addition at 25 ± 1°C and 60 ± 5% relative humidity. For cascade impactor analysis, the powder sample was filled accurately into a hard gelatin size 2 capsule (San Tronic Medical Devices, Selangor, Malaysia). The capsule was placed in the central compartment of a dry powder inhaler (HandiHaler, Boehringer Ingelheim, Germany; Supplementary Figure 1) and pierced/actuated in the cascade impactor to release the powder at an air flow rate of 48 L/min for 5s, corresponding to a 4 kPa pressure drop similar to those of the human lungs.[12] The emitted powder from the capsule was collected carefully from all the parts and stages of the cascade impactor using acetonitrile and methanol (4:1) co-solvent. The samples were sonicated (Elma, Germany) for 6 repetitive cycles of 10 min each with 10-min resting intervals followed by centrifugation (Heraeus Labofuge 200, Thermo Scientific, USA) at 2000 rpm for 10 min to collect the supernatant. The supernatant was filtered using a 0.45 μm nylon syringe filter (Agilent, Germany). The filtered samples were subjected to High Performance Liquid

Chromatography (HPLC) analysis to assess the contents of SX and FP at different parts and stages of ACI. All experiments were conducted in triplicates and the results were averaged.

The emitted dose (ED) was defined as the sum of mass collected from the mouthpiece, induction port, pre-separator and all stages. The deposited dose (DD) was defined as the sum of the mass collected from stage 2 to stage F. Percent inhaled (PI) was calculated as DD over total dose (TD), while percent dispersed (PD) was calculated as the ED over TD. Fine particle doses (FPD) were calculated at cut-off stage diameters <4.5 μm, <3.6 μm, and >0.5 μm but <3.6 μm. The fine particle fraction (FPF) was expressed as the percentage of FPD over ED and the respirable fraction (RF) was expressed as the percentage of FPD to the DD. The mass median aerodynamic diameter (MMAD) represented the particle size at the 50% cumulative mass weighted distribution (S_{50}). The geometric standard deviation (GSD) was calculated as the square root of the ratio of the particle size at the 84.13^{th} percentile to the 15.87^{th} percentile. The aerosolization and inhalation parameters of drugs were calculated using the following equations:

$$\mathrm{PI}(\%) = \mathrm{DD}/\mathrm{TD} \times 100 \tag{4}$$

$$\mathrm{PD}(\%) = \mathrm{ED}/\mathrm{TD} \times 100 \tag{5}$$

$$\mathrm{FPF}(\%) = \mathrm{FPD}/\mathrm{ED} \times 100 \tag{6}$$

$$\mathrm{RF}(\%) = \mathrm{FPD}/\mathrm{DD} \times 100 \tag{7}$$

$$\mathrm{MMAD} = S_{50} \tag{8}$$

$$\mathrm{GSD} = \sqrt{S84.13/S15.87} \tag{9}$$

HPLC Analysis

The quantification of SX and FP was performed using the HPLC technique (Agilent Technologies 1100 series, Agilent Technologies, USA). Agilent Zorbax SB-C18 reversed-phase column (4.6 × 250 mm, 5 μm; Agilent, Germany) was used as the stationary phase. The mobile phase consisted of acetonitrile and methanol (80:20 v/v). It was filtered using cellulose nitrate membrane (pore size 0.45 μm; Agilent, Germany) prior use. The flow rate of mobile phase was 0.5 mL/min for SX and 1.0 mL/min for FP. The column compartment temperature was kept at 40°C. The sample injection volume was 20 μL. The UV detector wavelength was set at 220 nm for SX and 232 nm for FP.

Fourier-Transform Infrared Spectroscopy (FTIR) Analysis

FTIR analysis was performed to analyze the interaction behaviour of hydrophobic drug with magnesium stearate, lactose-PEG 3000 microparticles or both. FP, magnesium stearate, lactose-PEG 3000 microparticles and various powder blends (2 mg) were ground with potassium bromide (78 mg, FTIR grade; Aldrich, Germany) and compressed into translucent discs using hydraulic pellet press (Specac Ltd., UK). The disc was scanned across a wavenumber range of 400 to 4000 cm^{-1} at a resolution of 4 cm^{-1} (Spectrum RX1 FTIR system, Perkin Elmer, USA). Each sample was tested in triplicates and the results were averaged.

In vivo Study

Healthy male Sprague Dawley rats (body weight = 200–250 g/rat) were obtained from the Laboratory Animal Facility and Management (LAFAM), Universiti Teknologi MARA (UiTM), Malaysia. The rats were individually housed in ventilated cages at 25°C with a relative humidity of 55 ± 5% and maintained on a 12 h light/dark cycle. They had unrestricted access to pelletized food (Gold Coin Enterprise, Malaysia) and de-ionized water ad libitum. Corncob was utilized as the bedding material due to its high absorbency, capacity to reduce ammonia odour and cost-effectiveness. The rats were acclimated for 7 days and underwent 12-h fasting period before conducting the experiment. Throughout the

study, compressed tissue-paper balls were provided in each cage to help reducing stress and promote typical behaviour of rats. All the experimental procedures were approved by institutional Committee on Animal Research and Ethics (UiTM CARE: 434/2023), meeting the American Veterinary Medical Association guidelines.

Pharmacokinetics

The rats were randomly assigned to three groups (n = 5/group). Group 1 received neat SX at a dose of 200 µg/kg. Group 2 received neat FP at a dose of 1000 µg/kg. Group 3 received dry powder formulation containing SX (200 µg/kg) and FP (1000 µg/kg). All dry powder samples were administered via the inhalation route. The rats were anaesthetised by intra-peritoneal injection of Zoletil 50 at 0.1 mL/100 g body weight. They were placed in a tilted upright position. An inhalation device, consisting of 5-mL syringe injector connected to a powder chamber made of a silicone tubing (internal diameter = 2.1 mm; length = 45 mm; Supplementary Figure 2), was inserted into the mouth cavity of rats with the edge of the silicone tubing reaching the inner opening of the mouth cavity. The powder sample was injected with 5 mL of air into the mouth cavity. At 0.3, 1, 2, 6, 8, 16 and 24 h, the blood was withdrawn (0.2 mL/interval) from the rat tail vein and collected in heparinized tubes (Reflotron, Roche, Germany) followed by immediate centrifugation (Z216MK, Hermle Labortechnik GmbH, Germany) at 5000 rpm for 30 min to separate the plasma from blood cells. The plasma was stored at −20°C until further drug content analysis by liquid chromatography-mass spectrometry (LC-MS) method. The rats were sacrificed by carbon dioxide euthanasia at the end of experiments.

Drug Retention

Three groups of rats (n = 5/group) were similarly treated with powder samples using the protocol outlined in the pharmacokinetics assessment section. After 2 h of inhalation, the rats were sacrificed by decapitation and the lungs were harvested and sectioned into the upper and lower regions. The upper and lower regions of lung (Supplementary Figure 3) were homogenized with phosphate buffer saline (pH 7.4) and methanol mixture at a volume ratio of 4:1 to extract the SX and FP. The homogenate was centrifuged with supernatant subjected to LC-MS analysis of drug content.

LC-MS Analysis

A 1260 liquid chromatography system coupled to a 6420 triple quadrupole mass spectrometer with electrospray ionization (ESI) interface was used (Agilent Technologies, Germany). The chromatography separation was performed at 35°C on a Zorbax Eclipse Plus C18 column (100 mm × 4.6 mm, 3.5 µm particle size; Agilent Technologies, Germany). The mobile phase consisted of 0.1% formic acid and 5 mM ammonium formate in water (solvent A) and 0.1% formic acid and 5 mM ammonium formate in acetonitrile (solvent B). The following gradient profile was adopted: 5% B (95% A), linear gradient to 95% B (5% A) in 5 min followed by 5% B (95% A) for 1 min, with a total run time of 10 min. The mobile phase flow rate was 0.45 mL/min with a sample injection volume of 1 µL. The mass spectrometer was operated in positive mode with the following parameter settings: nitrogen drying gas temperature at 350°C and with a flow rate of 11 mL/min; nebulizer pressure of 40 psi; capillary voltage of 3.5 kV. Quantification was performed in the positive ionization mode using multiple reaction monitoring (MRM) transitions of 416.3 to 232.3 m/z (collision energy 20 eV) and 501.2 to 313.3 m/z (collision energy 17 eV) as quantifier ions for SX (limit of detection: 0.006 µg/mL, limit of quantification: 0.02 µg/mL) and FP (limit of detection: 0.07 µg/mL, limit of quantification: 0.25 µg/mL), respectively. Data were processed with MassHunter Workstation software version B.06.00 (Agilent Technologies, Germany).

Pharmacodynamics

The rats (n = 5/group) were randomly divided into five groups: group I (normal control), group II (OVA-sensitized control), group III (OVA + neat SX 200 µg/kg), group IV (OVA + neat FP 1000 µg/kg) and group V (OVA + dry powder formulation). The asthmatic rat model was developed by sensitizing each rat on day 1 and 8 with OVA (100 µg) along with aluminium hydroxide (5 mg) emulsified in phosphate buffer saline (1 mL) administered via the intra-peritoneal injection. On days 15, 16 and 17, the rats were further challenged with OVA (50 µg) by inhalation. On days 16, 17 and 18, the rats were treated with the powder samples following the protocol outlined in the pharmacokinetics assessment. On day 19, the bronchoalveolar lavage fluid (BALF) was collected and subjected to cytokine characterization (IL-4, IL-5, IL-9 and IL-13) using enzyme-linked immunoassay (ELISA) kits (ELK, Biotechnology, USA). The lung lobes were

harvested and subjected to histopathological analysis using hematoxylin and eosin staining (Hematoxylin-Eosin Stain kit, Solarbio, China). For BALF collection, ice cold phosphate buffer saline (1 mL) was inserted into the trachea three times using a 16-gauge catheter. The recovered BALF was centrifuged at 2000 rpm for 10 min. The supernatant was stored at −80°C for cytokine characterization. The pellet was resuspended in 0.1 mL phosphate buffer saline, and slides were prepared using Diff quick staining kit (Diff-Quick Stain Kit, Solarbio China) and examined under light microscope (DM 2000, Leica, Germany) for blood cell count analysis.

Statistical Analysis

Results were represented as mean and standard deviation of at least three experiments. Student's *t*-test and polynomial correlation were applied when applicable and a statistically significant difference was denoted by $p < 0.05$.

Results and Discussion

Lactose-PEG 3000 Microparticles

Size

Preliminary experiments showed that spray drying of lactose solution alone without PEG 3000 led to the formation of hygroscopic and aggregative mass. The waxy PEG 3000 was essential to maintain the crystalline characteristics of lactose microparticles, preventing them from excessive moist wetting and introducing free flow property.[12,19–21] Overall, lactose-PEG 3000 microparticles were characterized by d_{50} values ranging between 5 µm and 50 µm (Table 1). With reference to F1, an increase in particle size in F2 was brought about by high processing temperature which could promote PEG 3000 softening (PEG 3000 melting point = 63°C)[22] that bound the spray-dried particles into larger aggregates (Student's *t*-test, $p < 0.05$). Reduced PEG 3000 content and liquid feeding rate increased the atomization efficiency and decreased the binding propensity of particles. This resulted in F3 being characterized by smaller particle sizes than F1 (Student's *t*-test, $p < 0.05$). However, a further reduction in PEG 3000 content could translate to the availability of a higher water fraction during spray drying. The water removal process was less efficient and the available moist bound the particles into aggregates (F4) larger than F3 (Student's *t*-test, $p < 0.05$). With reference to F3, the reduced lactose content in F5 resulted in a higher PEG 3000 fraction freely available to bind the drying particles into larger aggregates. Ethanol is a well-known surfactant used in reducing the size of spray-dried particles.[23] An ethanol concentration as high as 30% can reduce the particle size of F4 to approximately 5 µm (F8). Nonetheless, ethanol-free lactose-PEG 3000 microparticles were preferred in terms of residual organic solvent toxicity, processing safety and product cost.

Pulmonary delivery of SX and FP targets at upper and lower respiratory tracts, respectively, for the treatment of bronchospasm and lung inflammation. F3 (5.87 ± 0.03 µm) was deemed workable for delivery of FP in the form of a physical blend. To produce larger lactose-PEG 3000 microparticles as SX carrier that impacts the upper lung, the liquid feeding rate of F3 production was raised to reduce the atomization efficiency, keeping the lactose and PEG 3000 content larger than those of F5 and F4, respectively. The formed F9 was characterized by a d_{50} of 9.71 ± 0.04 µm, approximately twice the particle size of F3 (Table 1).

Morphology

F3 and F9 were selected for subsequent study with reference to their particle sizes favourable for lower lung and upper lung targeting, respectively. Both F3 (Circ = 0.41 ± 0.12) and F9 (Circ = 0.48 ± 0.15) were non-spherical in shape (Figure 1a). Irregularly shaped particles experience an increased aerodynamic drag, which can facilitate their deposition in the respiratory tract.[24] The particulate surfaces of F3 (Ra = 66.79 ± 7.00 nm) and F9 (Ra = 76.79 ± 5.05 nm) were relatively rough. The irregular protrusions and valleys could provide a large specific surface area for drug binding (Table 1),[25] forming an inhalable physical blend.

Crystallinity

XRD spectra showed that both F3 and F9 were crystalline (Figure 1b), with characteristic lactose monohydrate sharp peaks at $2\theta = 19.70°$ and 19.96°, respectively. The crystallinity level of F9 (58.0 ± 0.8%) was higher than that of the F3 (54.8 ± 1.7%). The crystalline domains of the lactose-PEG 3000 microparticles were envisaged to exhibit lower surface

 https://doi.org/10.2147/DDDT.S582476

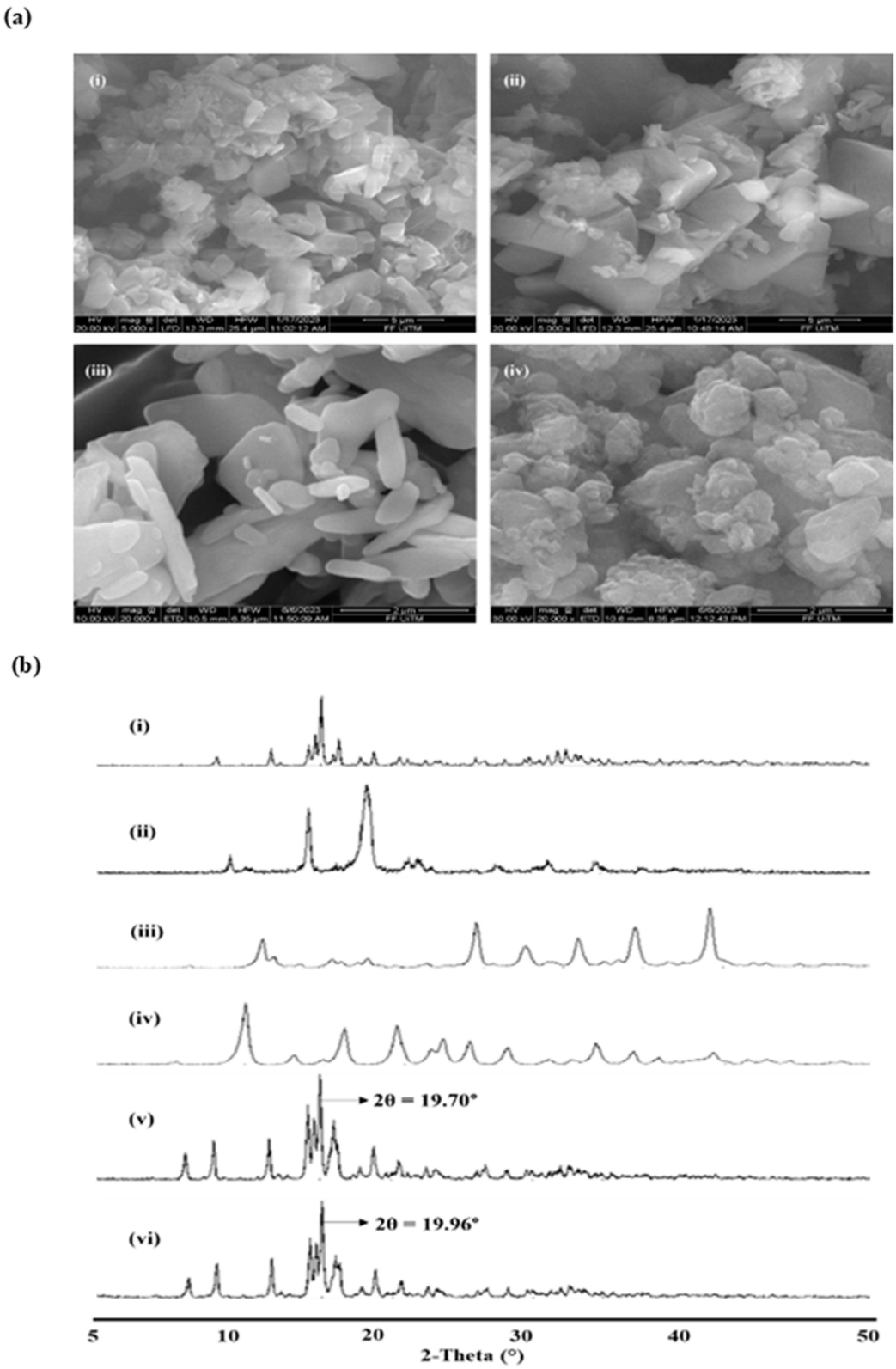

Figure 1 (**a**) SEM images of (i) F3, (ii) F9, (iii) SX and (iv) FP; (**b**) XRD spectra of (i) lactose monohydrate, (ii) PEG 3000, (iii) SX, (iv) FP, (v) F3 and (vi) F9.

energy. This could reduce the intermolecular forces between lactose-PEG 3000 carrier and the drug, facilitating the drug detachment from the carrier during the inhalation process.[26]

SX and FP

Both SX and FP were highly crystalline (Figure 1b). The crystallinity indices of SX and FP were 61.0 ± 0.2% and 63.9 ± 2.0%, respectively. They were irregular in shape (Circ: SX = 0.58 ± 0.35; FP = 0.78 ± 0.08; Figure 1a) with SX (Ra = 45.52 ± 5.36 nm; zeta potential = −10.1 ± 1.7 mV) appeared to have a rougher surface with a lower zeta potential than those of FP (Ra = 35.77 ± 5.10 nm; zeta potential = −20.7 ± 2.5 mV).

SX (d_{50} = 1.28 ± 0.03 μm; span = 1.48 ± 0.11) and FP (d_{50} = 2.37 ± 0.08 μm; span = 2.49 ± 0.01) had near submicron sizes suitable for pulmonary inhalation. Nonetheless, they were aggregative (SX: Carr's index = 34.0 ± 1.02%; Hausner ratio = 1.5 ± 0.01; FP: Carr's index = 43.0 ± 2.5; Hausner ratio = 1.7 ± 0.1). Physical blending of nanoparticles with microparticles with unlike surface properties has been demonstrated to mutually reduce their cohesiveness by disaggregating the nanoparticles via deposition onto the surfaces of microparticles, with the surface-deposited nanoparticles acting as glidants to reduce the aggregation tendency of microparticles.[19,27] Both F3 and F9 were characterized by poor flow properties (F3: ρ_b = 0.16 ± 0.01 g/cm^3, ρ_t = 0.21 ± 0.00 g/cm^3, Carr's index = 24.3 ± 4.5, Hausner ratio = 1.3 ± 0.1; F9: ρ_b = 0.18 ± 0.03 g/cm^3, ρ_t = 0.25 ± 0.01 g/cm^3, Carr's index = 28.5 ± 8.8, Hausner ratio = 1.4 ± 0.2). They were polydisperse in size and this could promote their particle aggregation tendency (Table 1). Despite F9 was larger in size than F3, it has a rougher surface morphology which contributed to interparticle interaction and poorer flow than F3. Physical blending of both lactose-PEG 3000 microparticles with drugs could have led to improved flowability and inhalation performance. To examine this, the subsequent study evaluated the aerosolization and inhalation patterns of individual drugs as well as their blends with lactose-PEG 300 microparticles using the cascade impactor technique.

Physical Blend of Lactose-PEG 3000 Microparticles and Drugs

Preliminary aerosolization and inhalation experiments with SX suggested that F3 and F9 provided similar pulmonary drug delivery profiles with F3 (PD = 86.9 ± 8.0%, PI = 39.2 ± 2.4%, FPF: 30.3 ± 1.9%) being marginally better than F9 (PD = 84.9 ± 13.0%; PI = 36.1 ± 8.4%; FPF = 26.1 ± 2.2%) in SX fractions (F3: 12.92 ± 3.89%; F9: 9.46 ± 1.41%) collected between stages 3 (trachea and primary bronchi) and 5 (terminal bronchi) which represented its intended respiratory target (Student's *t*-test, p ~ 0.05). On this note, F9 was excluded in the subsequent study despite it was initially hypothesized as a favourable carrier for the upper respiratory tract targeting of SX. F3 was adopted as the model drug carrier. Targeting of SX to the upper lung and FP to the lower lung was instead introduced by depositing FP adjacent to the surfaces of lactose-PEG 3000 microparticles (interior layer), with SX forming the exterior layer in contact with the immediate lung environment. Aerosolization and inhalation of this physical blend was expected to result in early SX release followed by delayed FP dispersion along the respiratory tract.

Neat SX and FP were characterized by poorer aerosolization and inhalation performance compared to their physical blends with varying contents of F3 (Table 2a). The dispersion and inhalation percentages of FP tended to be lower than SX as suggested by their Carr's index and Hauner ratio values, despite FP comprising larger particles with smoother surfaces that expressed a higher magnitude of zeta potential, which are features typically associated with better powder flowability.[12] A greater deviation from sphericity and the rod-like shape of SX could be responsible for its higher inhalation capacity. Such geometry has been shown to facilitate the aerodynamic flow of particles along the air stream in the respiratory tract.[28]

Physical blending of drugs with 20 mg of F3 led to higher aerosolization and inhalation extent than blends with 10, 40 and 80 mg F3 (Table 2a and Supplementary Equation 1). An excessively low F3 fraction translated to inadequate microcarrier for surface deposition by drugs. The freely available drug particles tended to aggregate among themselves or adhere to the capsule wall. Excessively high F3 fraction, on the other hand, might undergo inadequate surface coverage by drugs. The glidant effects of drugs on F3 could be insufficient to prevent them from aggregation. Thus, the form powder mixture exhibited poor flow properties (20 mg F3: Carr's index = 26.0 ± 1.0, Hauner ratio = 1.3 ± 0.0 vs 40 mg F3: Carr's index = 30.0 ± 1.5, Hausner ratio = 1.4 ± 0.0; 80 mg F3: Carr's index = 34.0 ± 0.5, Hausner ratio = 1.5 ± 0.0).

https://doi.org/10.2147/DDDT.S582476

https://doi.org/10.2147/DDDT.S582476

Table 2 Aerosolization and Inhalation Profiles of (a) Neat SX and FP and Their Physical Blends with Different F3 Masses, (b) SX and FP in Physical Blends with 20 mg F3 and Varying Contents of Magnesium Stearate, and (c) SX and FP in Their Physical Blends with 20 mg F3 and 5% Magnesium Stearate with Drugs First Individually Added to F3-Magnesium Stearate Mix

(a)										
Parameter	**Neat SX**	**Neat FP**	**F3 Mass (mg)**							
			80		**40**		**20**		**10**	
			SX	**FP**	**SX**	**FP**	**SX**	**FP**	**SX**	**FP**
MMAD (μm)	2.83 ± 0.73	1.74 ± 0.20	2.04 ± 0.36	1.45 ± 0.14	1.24 ± 0.30	1.98 ± 0.90	2.38 ± 0.16	1.69 ± 0.20	2.71 ± 0.50	1.46 ± 0.20
GSD	1.84 ± 0.09	3.10 ± 0.02	2.00 ± 0.20	1.90 ± 0.10	1.35 ± 0.15	1.17 ± 0.01	2.26 ± 0.10	1.78 ± 0.23	3.0 ± 1.10	1.43 ± 0.30
TD (μg)	**200**	**1000**	**200**	**1000**	**200**	**1000**	**200**	**1000**	**200**	**1000**
ED (μg)	118.11 ± 26.40	475.10 ± 59.15	140.90 ± 4.80	547.0 ± 76.62	148.70 ± 150	674.60 ± 22.0	179.2 ± 6.95	873.65 ± 16.0	132.10 ± 8.50	582.09 ± 70.0
DD (μg)	48.42 ± 21.0	141.68 ±33.50	70.90 ± 6.14	259.97 ± 30.04	75.60 ± 7.40	300.50 ± 10.0	90.58 ± 4.43	432.31 ± 29.0	61.71 ± 2.50	234.40 ± 35.02
PD (%)	59.05 ± 13.50	47.51 ± 5.69	70.95 ± 2.50	54.76 ± 7.50	74.39 ± 7.50	67.41 ± 4.56	89.60 ± 3.60	87.36 ± 3.50	66.08 ± 5.0	58.20 ± 9.50
PI (%)	24.21 ± 11.35	14.16 ± 2.90	35.45 ± 1.40	25.90 ± 3.70	37.81 ± 3.80	30.05 ± 1.09	45.29 ± 2.23	43.23 ± 3.30	30.86 ± 1.10	23.44 ± 5.02
Particles < 4.5 μm										
FPD (μg)	32.50 ± 10.60	94.42 ± 32.0	41.19 ± 3.80	159.80 ± 34.0	43.04 ± 8.10	159.40 ± 8.0	57.19 ± 1.12	253.44 ± 15.92	40.79 ± 3.50	143.70 ± 16.50
FPF (%)	27.01 ± 2.60	19.51 ± 4.20	29.07 ± 2.0	28.90 ± 2.10	28.83 ± 2.50	23.70 ± 2.0	31.97 ± 1.58	29.02 ± 1.50	30.83 ± 0.80	24.75 ± 5.0
RF (%)	70.16 ± 9.0	65.50 ± 7.50	58.20 ± 4.90	61.10 ± 5.10	56.59 ± 7.42	53.0 ± 0.50	63.21 ± 1.85	58.92 ± 5.50	66.08 ± 5.90	61.18 ± 2.95
Particles < 3.6 μm										
FPD (μg)	26.89 ± 8.80	54.65 ± 3.10	32.19 ± 4.80	107.20 ± 19.0	32.90 ± 8.0	99.50 ± 3.0	45.81 ± 3.90	150.16 ± 11.51	34.45 ± 4.50	93.46 ± 15.20
FPF (%)	22.43 ± 2.0	11.57 ± 0.70	22.70 ± 3.50	19.47 ± 0.70	22.15 ± 4.50	14.70 ± 1.0	25.66 ± 3.20	17.24 ± 1.97	25.98 ± 1.50	16.11 ± 3.0
RF (%)	58.57 ± 10.0	39.67 ± 7.0	45.41 ± 5.50	41.16 ± 2.50	43.28 ± 7.89	33.10 ± 0.05	50.50 ± 2.25	37.95 ± 3.80	55.82 ± 3.50	39.94 ± 1.50
0.5 μm < Particles < 3.6 μm										
FPD (μg)	22.45 ± 7.40	50.18 ± 2.70	28.97 ± 2.0	101.80 ± 12.0	27.81 ± 7.50	94.40 ± 6.0	39.45 ± 2.80	138.91 ± 6.19	29.33 ± 2.90	86.81 ± 17.0
FPF (%)	18.72 ± 1.80	10.63 ± 0.70	20.45 ± 2.10	18.44 ± 0.70	18.83 ± 5.10	14.05 ± 1.40	22.06 ± 2.30	15.93 ± 1.20	22.15 ± 0.60	14.91 ± 2.32
RF (%)	48.89 ± 8.70	36.44 ± 6.50	40.78 ± 5.60	38.96 ± 2.70	36.71 ± 9.50	31.37 ± 1.0	43.54 ± 2.59	32.31 ± 3.50	47.52 ± 4.60	36.90 ± 1.40

(b)								
Parameter	**Magnesium Stearate Only**		**Magnesium Stearate Content (%w/w)**					
			2.5		**5**		**10**	
	SX	**FP**	**SX**	**FP**	**SX**	**FP**	**SX**	**FP**
MMAD (μm)	2.80 ± 0.15	1.57 ± 0.61	2.50 ± 0.28	1.71 ± 0.20	2.80±0.01	1.74±0.16	2.55±0.02	1.31±0.03
GSD	4.90±0.22	1.73±0.18	4.20±1.20	1.55±0.11	3.60±0.15	1.81±0.20	2.60±0.09	1.48±0.10
TD (μg)	**200**	**1000**	**200**	**1000**	**200**	**1000**	**200**	**1000**
ED (μg)	113.70±2.42	556.30±47.30	155.50±4.0	875.85±8.10	160.76±3.70	882.74±17.0	173.49±4.60	893.48±5.10
DD (μg)	42.50±2.63	206.01±29.80	85.16±10.05	388.08±24.50	80.72±5.10	448.07±16.50	79.06±6.60	375.49±14
PD (%)	56.85±1.21	55.63±9.40	77.70±1.80	87.58±0.84	80.38±2.0	88.27±1.80	86.74±2.40	89.24±5.70
PI (%)	21.29±1.31	20.60±5.90	42.50±3.05	38.80±2.40	40.36±2.50	44.80±1.60	39.53±6.80	37.54±4.0
Particles < 4.5 μm								
FPD (μg)	28.90±4.36	128.90±45.0	50.44±0.06	226.48±11.50	58.71±1.75	298.56±17.0	53.11±1.20	224.36±16.10
FPF (%)	25.34±3.29	22.40±4.27	32.45±0.80	25.85±1.120	36.51±0.50	34.0±1.50	30.61±1.89	25.14±1.90
RF (%)	67.48±6.07	61.41±4.05	59.54±0.01	58.39±0.58	72.84±2.45	66.63±2.30	67.17±0.40	59.75±4.50
Particles < 3.6 μm								
FPD (μg)	23.49 ± 3.38	72.09 ± 23.20	39.34 ± 0.01	162.59 ± 23.50	47.33 ± 0.95	206.86 ± 9.90	40.72 ± 1.20	150.54 ± 10.0
FPF (%)	20.60 ± 2.53	12.59 ± 2.15	25.30 ± 0.60	18.54 ± 2.50	29.44 ± 0.20	23.43 ± 0.90	23.47 ± 1.60	16.86 ± 1.01
RF (%)	54.80 ± 4.54	34.50 ± 1.59	46.43 ± 3.20	41.68 ± 3.40	58.75 ± 3.0	46.16 ± 1.60	51.50 ± 0.70	40.09 ± 1.20
0.5 μm < Particles < 3.6 μm								
FPD (μg)	21.00 ± 3.33	70.48 ± 24.10	32.70 ± 2.31	147.96 ± 28.0	40.57 ± 1.50	197.64 ± 11.80	34.08 ± 1.20	147.29 ± 8.70
FPF (%)	18.41 ± 2.53	12.28 ± 2.24	21.08 ± 1.90	16.86 ± 3.20	25.23 ± 0.50	22.39 ± 0.90	19.64 ± 1.50	16.50 ± 0.50
RF (%)	49.01 ± 4.79	33.64 ±1.95	38.82 ± 5.50	37.80 ± 5.20	50.34 ± 1.90	44.11 ± 1.70	43.11 ± 0.80	39.23 ± 2.20

(*Continued*)

https://doi.org/10.2147/DDDT.S582476

Table 2 (Continued).

(c)		
Parameter	**Dry Powder Formulation**	
	SX	**FP**
MMAD (μm)	3.44 ± 0.18	2.43 ± 0.7
GSD	6.10 ± 0.13	2.67 ± 0.21
TD (μg)	**200**	**1000**
ED (μg)	164.56 ± 5.19	905.11 ± 28.12
DD (μg)	80.69 ± 4.37	446.96 ± 28.51
PD (%)	82.28 ± 2.59	90.51 ± 2.81
PI (%)	40.34 ± 2.18	44.69 ± 2.85
Particles < 4.5 μm		
FPD (μg)	62.74 ± 2.01	312.53 ± 22.76
FPF (%)	38.12 ± 0.23	34.50 ± 1.42
RF (%)	77.83 ± 1.66	69.90 ± 0.80
Particles < 3.6 μm		
FPD (μg)	52.28 ± 1.57	236.97 ± 20.93
FPF (%)	31.77 ± 0.29	26.14 ± 1.47
RF (%)	64.86 ± 1.64	52.94 ± 1.44
0.5 μm < Particles < 3.6 μm		
FPD (μg)	38.11 ± 1.67	198.02 ± 11.22
FPF (%)	23.20 ± 1.72	21.86 ± 0.55
RF (%)	47.43 ± 4.37	44.32 ± 0.37

https://doi.org/10.2147/DDDT.S582476

Effects of Magnesium Stearate

Using 20 mg F3 admixed with drugs, the lactose-PEG 3000 microparticles fraction was relatively higher than drugs. Lactose-PEG 3000 microparticles with limited surface-deposited drugs might be aggregative. On this note, magnesium stearate was introduced as the lubricant to F3 prior to addition of drugs. Magnesium stearate was characterized by a d_{50} of 4.93 ± 0.13 μm. Based on the particle size attribute, it was considered capable of acting as a drug carrier, similar to F3. Density analysis nonetheless showed that the introduction of magnesium stearate to drugs (~20 mg powder mass) greatly reduced the flowability of powder (Carr's index = 58.0 ± 4.0, Hausner ratio = 2.4 ± 0.2). This could be due to excessive hydrophobic interaction between the drugs (SX: $P_{o/w}$ = 3.26; FP: $P_{o/w}$ = 3.4)[29,30] and magnesium stearate ($P_{o/w}$ = 7.15)[31] leading to the formation of aggregative mass. The unsuitability of magnesium stearate as drug carrier was further demonstrated by the aerosolization and inhalation analysis of drugs admixed with the lubricant (Table 2b). In contrast, the introduction of 5% magnesium stearate to 20 mg of F3 admixed with drugs improved flowability (Carr's index = 24.5 ± 2.50, Hausner ratio = 1.3 ± 0.0). Promotion of powder flowability required magnesium stearate to act as the lubricant of F3 instead of as the carrier of drugs.

Using 5% magnesium stearate, the FPFs of SX and FP admixed F3 reachable to upper and lower lungs increased (Table 2b and Supplementary Equation 2). Improved powder flowability promoted drug aerosolization and inhalation. The inhalation percentage of FP appeared to increase more substantially than that of SX through the intervention of magnesium stearate. The overall improvement in drug aerosolization and inhalation was not expectedly high. This could be associated with the tendency of magnesium stearate to hydrophobically interact with drugs into larger particles, as inferred by poorer powder flow and reduced FPF at 10% magnesium stearate content due to enhanced hydrophobic interactions with drugs.

FP was characterized by sharp FTIR peaks representing C=O at 1744.27 ± 0.01 cm^{-1}, thioester carbonyl at 1701.76 ± 0.02 cm^{-1}, ketone carbonyl at 1662.47 ± 0.01 cm^{-1}, C=C at 1613.93 ± 0.02 cm^{-1}, and O-H at 3327.0.4 ± 0.02 cm^{-1} (Figure 2). In the case of F3, FTIR peaks were observed at 1421.91 ± 0.00 cm^{-1} depicting C-O-H, 1655.26 ± 0.12 cm^{-1} denoting ketone carbonyl, and 2900.79 ± 0.02 cm^{-1} attributed to C-H. Magnesium stearate was characterized by peaks at 1577.02 ± 0.03 cm^{-1} representing C=O, and at 2850.50 ± 0.15 cm^{-1} and 2919.25 ± 0.10 cm^{-1} denoting C-H. A blend of F3 with magnesium stearate yielded a FTIR spectrum with characteristic peaks of F3 and magnesium stearate expressed at 1656.37 ± 0.10 cm^{-1} and 1576.08 ± 0.06 cm^{-1} respectively (Figure 2). The introduction of hydrophobic FP resulted in the loss of characteristic FTIR peak of F3 (1655.26 ± 0.12 cm^{-1}) along with increased transmission and reduced wavenumber of the characteristic FTIR peak of magnesium stearate (1577.02 ± 0.03 cm^{-1} to 1575.33 ± 0.01 cm^{-1}; Student's *t*-test, $p < 0.05$) (Figure 2). The hydrophobic drug appeared to interact with the magnesium stearate by forming stronger bonds as reflected by the reduced wavenumber in the F3-magnesium stearate-FP blend within the magnesium stearate FTIR domain. Excessive magnesium stearate (10%) could then form strong aggregates with the hydrophobic drugs, thereby hampering their aerosolization and inhalation processes.

Effects of Particle Mixing Pattern

The introduction of magnesium stearate brought about a relatively more dispersible powder mixture (Table 2b; standard coefficient of variation (PD): 2.83 ± 1.85%) than those without magnesium stearate in general (Table 2a; standard coefficient of variation (PD): 6.64 ± 5.52%). SX and FP are hydrophobic drugs. The deposition of SX onto the F3-magnesium stearate mix after the addition of FP nonetheless could have rendered them experiencing a comparatively intense hydrophobic interaction and unavoidable powder aggregation (Figure 3a). As such, the F3-magnesium stearate mix was individually blended with each drug before combining them into a single dry powder formulation. The cascade impactor analysis indicated that such powder design yielded a higher FPF of SX ($FPF_{<4.5\ \mu m}$: 38.12 ± 0.23%) compared to the single-microcarrier formulation ($FPF_{<4.5\ \mu m}$: 36.51 ± 0.50%) (Student's *t*-test, $p < 0.05$; Figure 3b and Table 2c). More SX was attached to the F3-magnesium stearate mix and being inhaled throughout the respiratory tract. This was reflected by the reduced SX contents in the mouthpiece (5.70 ± 0.89%) compared to powder prepared from F3-magnesium stearate admixed with FP then SX (10.96 ± 2.23%) (Student's *t*-test, $p < 0.05$; Figure 3). The $FPF_{< 3.6\ \mu m}$ of FP, targeting at the lower lung, likewise was raised by the dual-microcarrier approach (Student's *t*-test, $p < 0.05$). Overall, the FPF of SX was greater than FP (Table 2c). This was aptly explained by SX's ability to deposit onto the

 https://doi.org/10.2147/DDDT.S582476

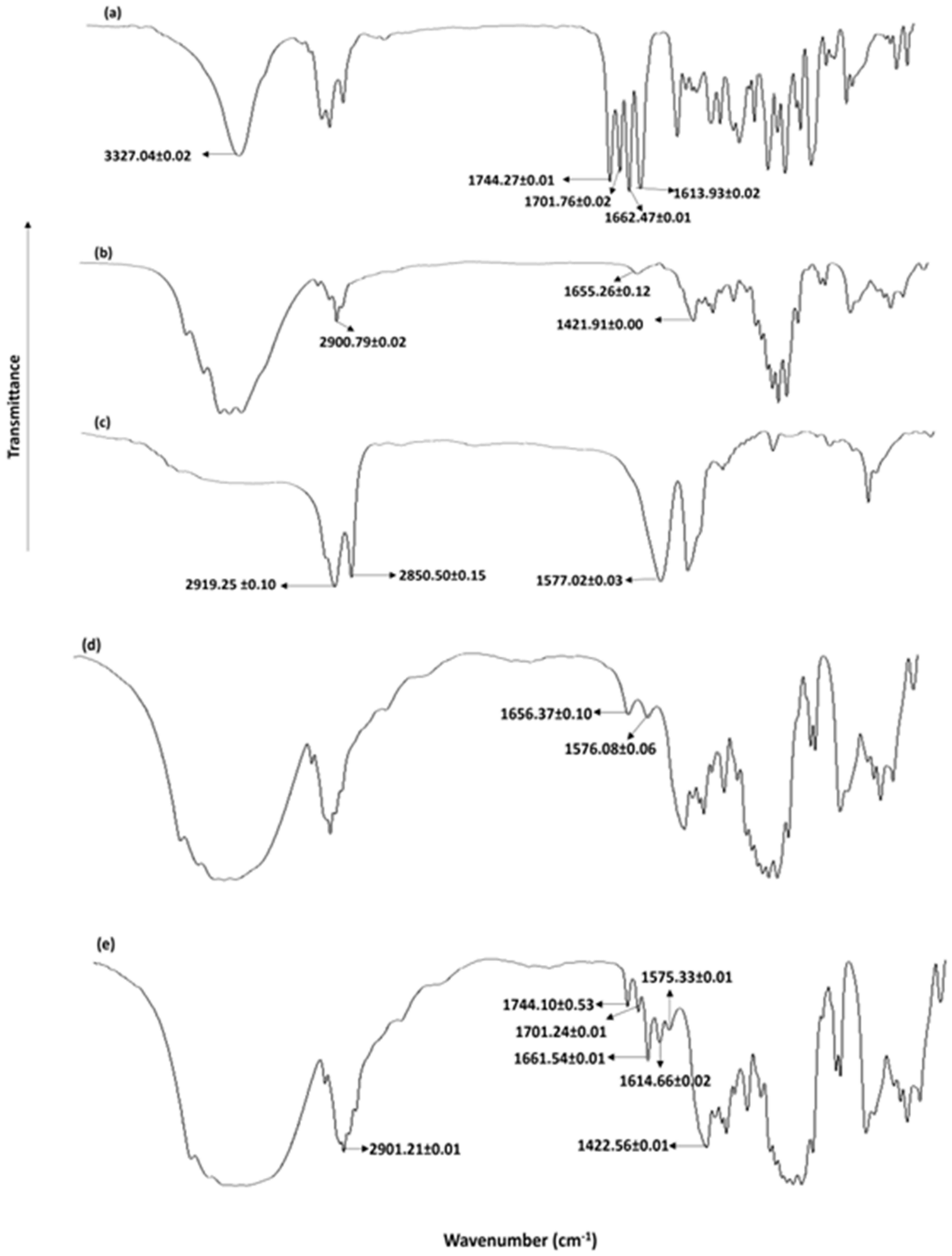

Figure 2 FTIR spectra of (**a**) neat FP, (**b**) F3, (**c**) magnesium stearate, (**d**) F3-magneisum stearate (5%) physical blend and (**e**) F3-magnesium stearate-FP physical blend.

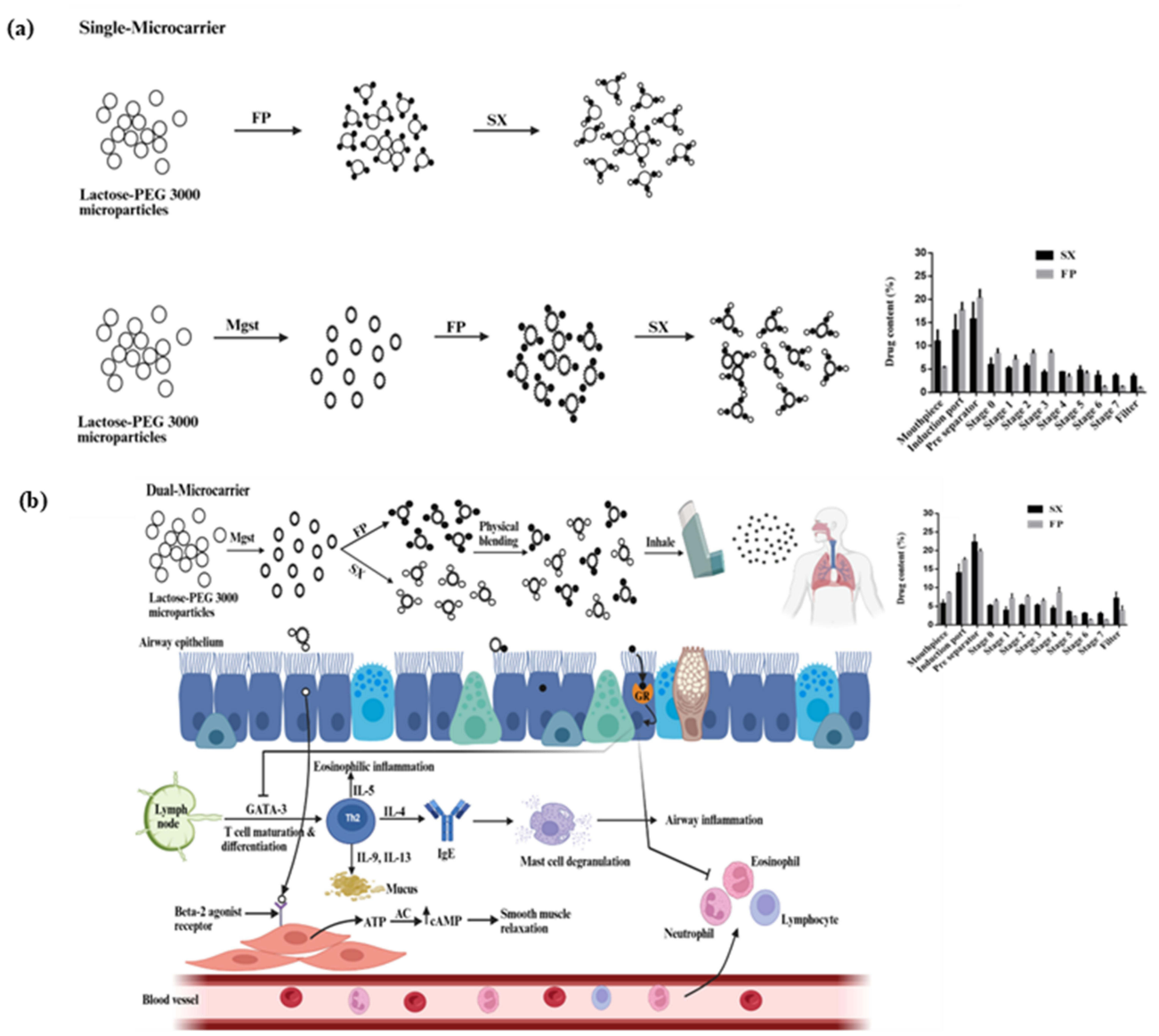

Figure 3 Schematic diagram of (**a**) single- vs (**b**) dual-microcarrier systems of SX and FP to overcome bronchospasm and lung inflammation.
Abbreviations: AC, adenyl cyclase; ATP, adenosine triphosphate; cAMP, cyclic adenosine monophosphate; GR, glucocorticoids receptor; IgE, immunoglobulin E; Mgst, magnesium stearate.

microcarrier due to its rougher particle surface with reduced zeta potential and relatively higher powder flowability than FP. The net inhalation performance of SX and FP was promoted by judicious microcarrier design. To further enhance drug delivery and targeting, drug particle physical characteristics are one potential parameter to modulate.

In vivo Study

Formulation of drugs using F3-magnesium stearate mix as their individual microcarrier improved drug retention throughout the lungs compared to neat drugs (Student's *t*-test, $p < 0.05$) with lung drug retention of FP being raised to a greater extent than SX (Table 3b). This formulation marginally changed the systemic distribution profiles of drugs with a rise in their plasma concentrations inferring that the drugs were flowing into deeper lungs (Figure 4 and Table 3a). With reference to systemic availability, FP was characterized by a higher plasma concentration than SX and this could be attributed to its higher molecular hydrophobicity[32] and availability at the alveolar interface. With improved lung drug retention accompanied by increased plasma drug levels, this dry powder formulation significantly reduced the cytokine

https://doi.org/10.2147/DDDT.S582476

Table 3 (a) Systemic Pharmacokinetic Profile Parameters and (b) Lung Drug Content Distribution

(a)				
Parameter	**Neat SX**	**Neat FP**	**Dry Powder Formulation**	
			SX	**FP**
C_{max} (μg/mL)	0.11 ± 0.01	0.23 ± 0.02	0.19 ± 0.03	0.26 ± 0.10
T_{max} (h)	2.0 ± 0.0	4.0 ± 0.0	2.0 ± 0.0	4.0 ± 0.0
AUC_{0-t} (μg/mL. h)	1.93 ± 0.01	4.24 ± 0.10	2.43 ± 0.08	4.30 ± 1.27
$AUC_{0-\alpha}$ (μg/mL. h)	5.47 ± 0.28	8.08 ± 1.15	8.71 ± 0.35	8.37 ± 0.97
$T_{1/2}$ (h)	38.32 ± 2.56	21.75 ± 1.82	54.25 ± 3.79	27.46 ± 8.69
(b)				
	Neat SX	**Neat FP**	**Dry Powder Formulation**	
			SX	**FP**
Upper region (μg/region)	3.55 ± 2.01	1.50 ± 0.97	12.04 ± 8.60	35.34 ± 20.24
Lower region (μg/region)	3.60 ± 2.23	2.97 ± 1.12	29.57 ± 5.50	67.13 ± 27.50
Total lung (μg/total lung)	7.16 ± 0.03	4.47 ± 0.73	41.62 ± 8.76	102.47 ± 15.89
Percent drug content retention (%)	14.32 ± 0.03	1.78 ± 0.73	83.24 ± 8.76	40.98 ± 15.89

Abbreviations: C_{max}, maximum drug concentration; T_{max}, time at which C_{max} occurs; AUC_{0-t}, area under curve from t = 0 to t = 24 h; $AUC_{0-\alpha}$, area under the curve from time of dosing to infinity; $T_{1/2}$, half-life.

IL-4 and IL-5 levels that were involved in IgE release and eosinophil-mediated inflammation (Figures 3b and 5a).[33] In addition, it suppressed IL-9 and IL-13 expression, which are responsible for mucus production leading to airway obstruction and ultimately into smooth muscle constriction (Figures 3b and 5a).[34]

Compared to healthy rats, the lungs of the asthmatic rats exhibited increased inflammatory cells infiltration, destruction of cellular structure and thickening of bronchiolar epithelial lining (Figure 5b). Neat drug treatment led to a slight improvement in lung tissue structure, though inflammatory cells infiltration and increased thickness of epithelial cells remained visible. Dry powder formulation, on the other note, reduced the inflammatory cells infiltration and epithelium thickness with lung histology resembling those of the healthy rats. Further, the dry powder formulation significantly reduced the lymphocyte, neutrophil and eosinophil counts (Figure 5c), suggesting a higher anti-inflammatory capacity than neat drugs.

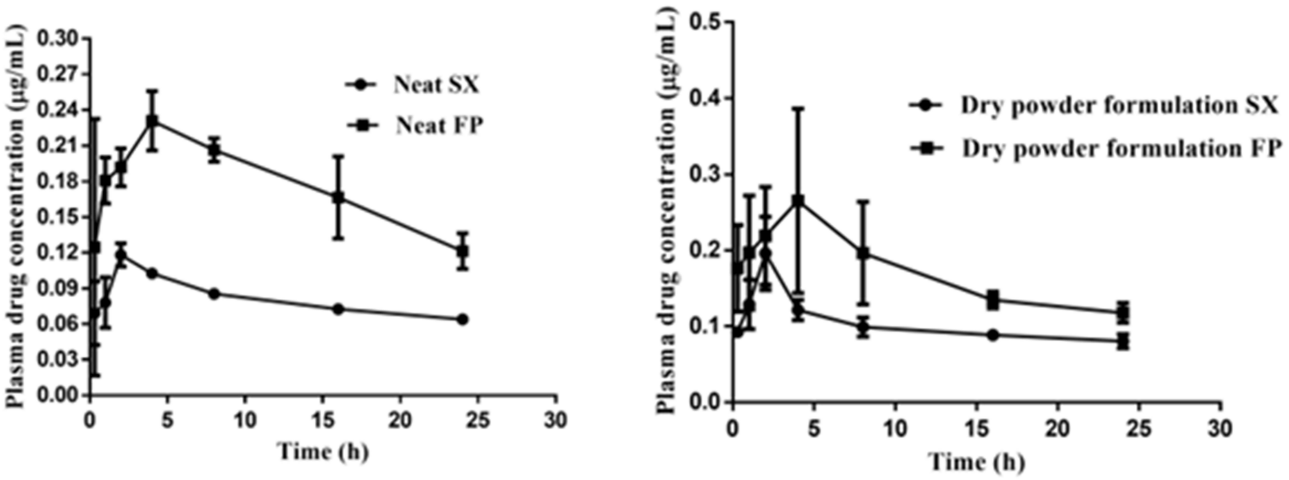

Figure 4 Systemic pharmacokinetic profiles of neat SX and FP and their physical blends with 20 mg F3 and 5% magnesium stearate with drugs first individually added to F3-magnesium stearate mix.

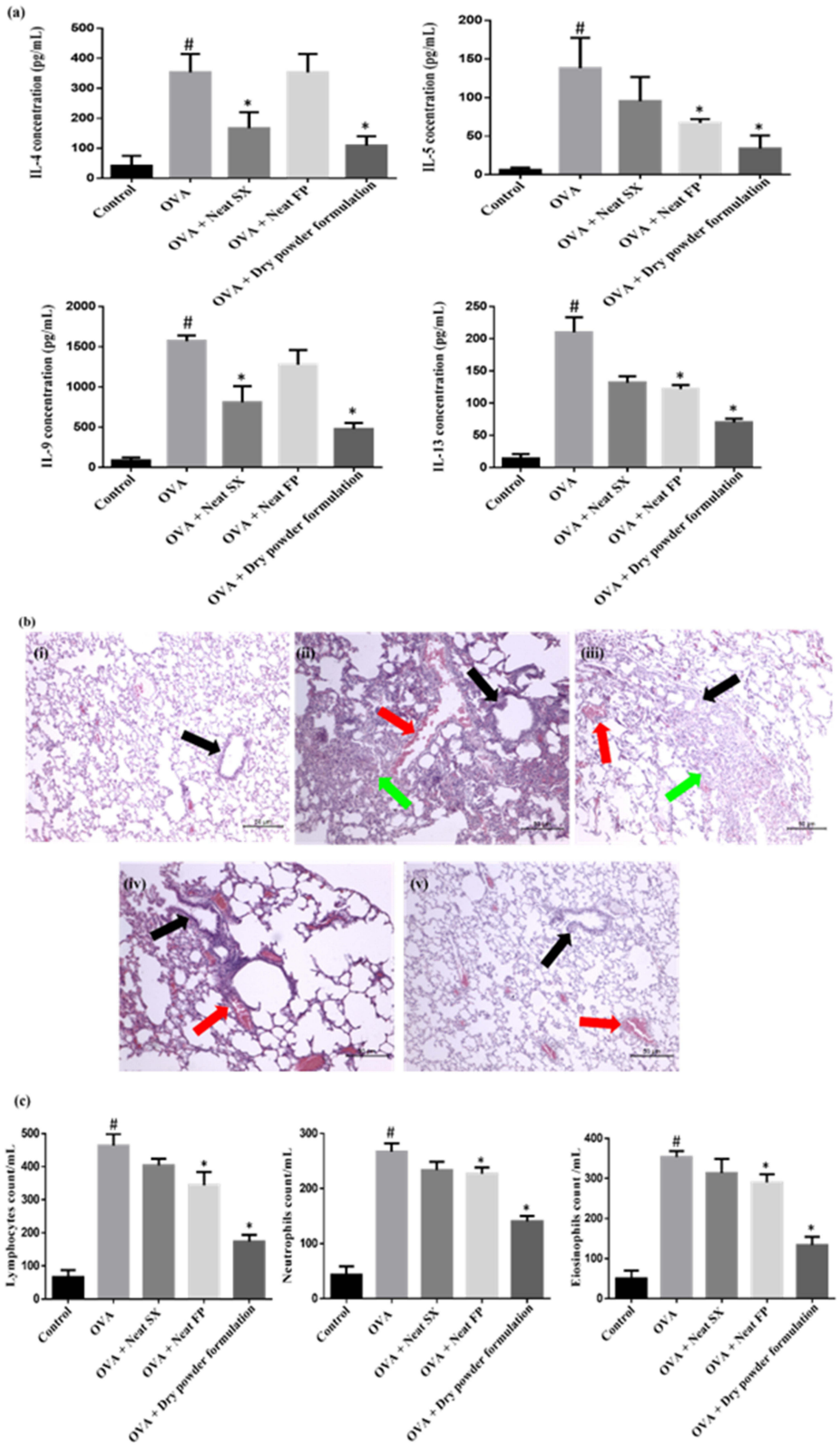

Figure 5 (**a**) profiles of IL-4, IL-5, IL-9 and IL-13 in BAL fluid of ovalbumin-induced asthmatic rats receiving no treatment, neat drugs and dry powder formulation against the healthy rats, (**b**) haematoxylin and eosin-stained lung tissue harvested on day 19 (i) control, (ii) OVA, (iii) OVA + neat SX, (iv) OVA + neat FP and (v) OVA + dry powder formulation (black arrow depicts bronchial epithelial thickness, red arrow depicts infiltration of inflammatory cells and green arrow depicts distorted alveolar space) and (**c**) lymphocyte, neutrophil and eosinophil count in lung tissue of ovalbumin-induced asthmatic rats receiving no treatment, neat drugs and dry powder formulation against the healthy rats. *denotes $p < 0.05$ against the asthmatic model; #denotes $p < 0.05$ against normal rats.

https://doi.org/10.2147/DDDT.S582476

Conclusion

Unlike single-carrier system, depositing the drugs onto different microcarriers followed by physical blending into a dry powder formulation enhanced FP inhalation into the lower lung due to the absence of an external SX barrier and reduced opportunistic hydrophobic aggregation between SX and magnesium stearate-FP previously deposited on the same microcarrier. This dual-microcarrier strategy promoted pulmonary delivery of both SX and FP ($FPF_{<4.5\ \mu m}$: SX = 38.12 ± 0.23%; FP = 34.50 ± 1.42%), outperforming commercial devices such as Accuhaler ($FPF_{<5\ \mu m}$: 19.6%), Revolizer ($FPF_{<5\ \mu m}$: 18.6%), and Lupihaler ($FPF_{<5\ \mu m}$: 11.4%)[35] as well as of SX delivery compared to Serevent Diskus and Seretide Diskus ($FPF_{<5\ \mu m}$: 20 to 25%).[36] Regardless of single- or dual-microcarrier systems, the introduction of magnesium stearate improved drug inhalation by reducing microcarrier aggregation. However, magnesium stearate alone was unable to act as a microcarrier and deliver the drugs without the intervention of lactose-PEG 3000 microparticles due to its tendency to develop excessive hydrophobic interaction with lipophilic SX and FP. Compared to neat drugs, the dual-microcarrier system increased pulmonary drug retention with only a marginal rise in systemic drug levels, owing to improved pulmonary inhalation. It reduced the infiltration of inflammatory lymphocytes, eosinophils and neutrophils, IL-4, IL-5, IL-9 and IL-13 release, and mitigated mucus production and bronchoconstriction which are essential in asthma control. Human lungs differ from those of rats anatomically and both humans and rats have different breathing patterns.[37] Humans tend to exhibit a greater variability in particle deposition due to asymmetrical lung anatomy. Future development requires clinical examination of the dry powder inhalation product. Future clinical translation of the dry powder inhalation product requires stringent quality control. A preliminary assessment of 12-month stability at a storage temperature of 25 ± 5°C and a relative humidity of 60 ± 5% suggested that the dual-microcarrier system had comparable powder flow properties against the freshly prepared sample (Carr's index = 22.3 ± 0.3; Hausner ratio = 1.3 ± 0.0). Real-time and accelerated stability studies are required to further confirm such quality attributes. Inhaler design has a strong bearing on the aerosolization and inhalation profiles of a dry powder.[38] To further raise the FPF of SX and FP, the interplay effects of inhaler design and powder formulation must be concurrently evaluated and optimized.

Abbreviations

AC, adenyl cyclase; ATP, adenosine triphosphate; AUC, area under curve; BALF, bronchoalveolar lavage fluid; cAMP, cyclic adenosine monophosphate; Circ, circularity; C_{max}, maximum drug concentration; DD, deposited dose; (d_{10}, d_{50} and d_{90}), volume weighted median diameter; $D_{[4,3]}$, volume weighted mean diameter; $D_{[3,2]}$, surface area weighted mean diameter; ED, emitted dose; ESI, electrospray ionization; ELISA, enzyme linked immunosorbent assay; FPD, fine particle dose; FPF, fine particle fraction; FP, fluticasone propionate; FTIR, Fourier transform infrared spectroscopy; GR, glucocorticoid receptor; GSD, geometric standard deviation; HPLC, high performance liquid chromatography; IgE, immunoglobulin; IL, interleukin; LAFAM, laboratory animal facility and management; LC-MS, liquid chromatography-mass spectrometry; Mg.st, magnesium stearate; MMAD, mass median aerodynamic diameter; MRM, multiple reaction monitoring; OVA, ovalbumin; PEG, polyethylene glycol; ρ_b, bulk density; ρ_t, tapped density; PI, percent inhaled; PD, percent dispersed; Ra, surface roughness; RF, respirable fraction; SEM, scanning electron microscopy; SX, salmeterol xinafoate; Th2, helper type 2; TD, total dose; $T_{1/2}$, half-life; T_{max}, time at which C_{max} occurs; XRPD, x-ray powder diffractometer.

Data Sharing Statement

The data is available upon request.

Acknowledgments

The authors wish to express their heart-felt gratitude to Universiti Teknologi MARA and Malaysian Cocoa Board for facility support, and Ministry of Higher Education (IMAP/1/2024/SKK16/UITM/1) for funding support.

Author Contributions

All authors made a significant contribution to the work reported, whether that is conceptualization, methodology, validation, resources, data curation, writing original draft, writing review and editing; gave final approval of the version to be published; agreed to submit the article in this journal; and agreed to be accountable for all aspects of the research work.

Disclosure

The authors declare no conflicts of interest in this work.

References

1. Yu Y, Ni M, Zheng Y, Huang Y. Airway epithelial-targeted nanoparticle reverses asthma in inhalation therapy. *J Control Release*. 2024;367:223–234. doi:10.1016/j.jconrel.2024.01.044
2. Dorscheid D, Gauvreau GM, Georas SN, et al. Airway epithelial cells as drivers of severe asthma pathogenesis. *Mucosal Immunol*. 2025;18 (3):524–537. doi:10.1016/j.mucimm.2025.03.003
3. Habib N, Pasha MA, Tang DD. Current understanding of asthma pathogenesis and biomarkers. *Cells*. 2022;11:2764. doi:10.3390/cells11172764
4. Akram MW, Wong TW. Translational hurdles in anti-asthmatic nanomedicine development. *Expert Opin Drug Deliv*. 2024;21:987–989. doi:10.1080/17425247.2024.2385092
5. Ainali NM, Xanthopoulou E, Michailidou G, Zamboulis A, Bikiaris DN. Microencapsulation of fluticasone propionate and salmeterol xinafoate in modified chitosan microparticles for release optimization. *Molecules*. 2020;25:3888. doi:10.3390/molecules25173888
6. Boboltz A, Kumar S, Duncan GA. Inhaled drug delivery for the targeted treatment of asthma. *Adv Drug Deliv Rev*. 2023;198:114858. doi:10.1016/j.addr.2023.114858
7. Usmani OS, Biddiscombe MF, Barnes PJ. Regional lung deposition and bronchodilator response as a function of β2-agonist particle size. *Am J Respir Crit Care Med*. 2005;172(12):1497–1504. doi:10.1164/rccm.200410-1414OC
8. Muralidharan P, Mallory EK, Malapit M, et al. Advanced design and development of nanoparticle/microparticle dual-drug combination lactose carrier-free dry powder inhalation aerosols. *RSC Adv*. 2020;10:41846–41856. doi:10.1039/D0RA07203F
9. Maneechotesuwan K, Yao X, Ito K, et al. Suppression of GATA-3 nuclear import and phosphorylation: a novel mechanism of corticosteroid action in allergic disease. *PLoS Med*. 2009;6:e1000076. doi:10.1371/journal.pmed.1000076
10. Fei Q, Bentley I, Ghadiali SN, Englert JA. Pulmonary drug delivery for acute respiratory distress syndrome. *Pulm Pharmacol Ther*. 2023;79:102196. doi:10.1016/j.pupt.2023.102196
11. Yue L, Zhang X, Zhao C, Chen R, Chen X, Rao L. Inhaled drug delivery: past, present, and future. *Nano Today*. 2023;53:101942. doi:10.1016/j.nantod.2023.101942
12. Alhajj N, Zakaria Z, Naharudin I, Ahsan F, Wenji L, Wong TW. Critical physicochemical attributes of chitosan nanoparticles admixed lactose-PEG 3000 microparticles in pulmonary inhalation. *Asian J Pharm Sci*. 2020;15:374–384. doi:10.1016/j.ajps.2019.02.001
13. Alyami MH, Dahmash EM, Ali DK, Alyami HS, AbdulKarim H, Alsudir SA. Novel fluticasone propionate and salmeterol fixed-dose combination nano-encapsulated particles using polyamide based on L-lysine. *Pharmaceuticals*. 2022;15:321. doi:10.3390/ph15030321
14. Amore E, Manca ML, Ferraro M, et al. Salmeterol Xinafoate (SX) loaded into mucoadhesive solid lipid microparticles for COPD treatment. *Int J Pharm*. 2019;562:351–358. doi:10.1016/j.ijpharm.2019.03.059
15. Dahmash EZ, Achkar NR, Ali DK, et al. Preclinical evaluation of novel synthesised nanoparticles based on tyrosine poly (ester amide) for improved targeted pulmonary delivery. *Sci Rep*. 2024;14:9845. doi:10.1038/s41598-024-59588-1
16. Khandouzi F, Daman Z, Gilani K. Optimized particle engineering of fluticasone propionate and salmeterol xinafoate by spray drying technique for dry powder inhalation. *Adv Powder Technol*. 2017;28:534–542. doi:10.1016/j.apt.2016.10.022
17. Pasero L, Susa F, Limongi T, Pisano R. A review on micro and nanoengineering in Powder-Based pulmonary drug delivery. *Int J Pharm*. 2024;659:124248. doi:10.1016/j.ijpharm.2024.124248
18. Rasul RM, Muniandy MT, Zakaria Z, et al. A review on chitosan and its development as pulmonary particulate anti-infective and anti-cancer drug carriers. *Carbohydr Polym*. 2020;250:116800. doi:10.1016/j.carbpol.2020.116800
19. Alhajj N, Naharudin I, Colombo P, Quarta E, Wong TW. Probing critical physical properties of lactose-polyethylene glycol microparticles in pulmonary delivery of chitosan nanoparticles. *Pharmaceutics*. 2021;13:1581. doi:10.3390/pharmaceutics13101581
20. Chidavaenzi OC, Buckton G, Koosha F. The effect of co-spray drying with polyethylene glycol 4000 on the crystallinity and physical form of lactose. *Int J Pharm*. 2001;216:43–49. doi:10.1016/S0378-5173(00)00693-1
21. Corrigan DO, Healy AM, Corrigan OI. The effect of spray drying solutions of polyethylene glycol (PEG) and lactose/PEG on their physicochemical properties. *Int J Pharm*. 2002;235:193–205. doi:10.1016/S0378-5173(01)00990-5
22. Dsouza AA, Shegokar R. Polyethylene glycol (PEG): a versatile polymer for pharmaceutical applications. *Expert Opin Drug Deliv*. 2016;13:1257–1275. doi:10.1080/17425247.2016.1182485
23. Yang DL, Liu RK, Wei Y, Sun Q, Wang JX. Micro-sized nanoaggregates: spray-drying-assisted fabrication and applications. *Particuology*. 2024;85:22–48. doi:10.1016/j.partic.2023.03.013
24. Chaurasiya B, Zhao YY. Dry powder for pulmonary delivery: a comprehensive review. *Pharmaceutics*. 2021;13:31. doi:10.3390/pharmaceutics13010031
25. Papadopoulou A, Gillissen JJJ, Tiwari MK, Balabani S. Effect of particle specific surface area on the rheology of non-brownian silica suspensions. *Materials*. 2020;13:4628. doi:10.3390/ma13204628
26. Ho R, Muresan AS, Hebbink GA, Heng JYY. Influence of fines on the surface energy heterogeneity of lactose for pulmonary drug delivery. *Int J Pharm*. 2010;388:88–94. doi:10.1016/j.ijpharm.2009.12.037

27. Ullah F, Shah KU, Shah SU, et al. Synthesis, characterization and in vitro evaluation of chitosan nanoparticles physically admixed with lactose microspheres for pulmonary delivery of montelukast. *Polymers*. 2022;14:3564. doi:10.3390/polym14173564
28. Pioch T, Fischer T, Schneider M. Aspherical, nano-structured drug delivery system with tunable release and clearance for pulmonary applications. *Pharmaceutics*. 2024;16:232. doi:10.3390/pharmaceutics16020232
29. Dogbe MG, Mafilaza AY, Eleuterio CV, Marques HC, Simoes S, Gaspar MM. Pharmaceutical benefits of fluticasone propionate association to delivery systems: in vitro and in vivo evaluation. *Pharmaceutics*. 2019;11:521. doi:10.3390/pharmaceutics11100521
30. Murnane D, Martin G, Marriott C. Validation of a reverse-phase high performance liquid chromatographic method for concurrent assay of a weak base (salmeterol xinafoate) and a pharmacologically active steroid (fluticasone propionate). *J Pharm Biomed Anal*. 2006;40:1149–1154. doi:10.1016/j.jpba.2005.09.028
31. Zhang Y, Liu T, Rahimi SK, Zhang F. A review of twin screw wet granulation mechanisms in relation to granule attributes. *Drug Dev Ind Pharm*. 2021;47:349–360. doi:10.1080/03639045.2021.1879844
32. Baghla R, Kapil SK, Kern R. Quantifying fluticasone propionate and salmeterol xinafoate with high sensitivity in human plasma. *DH Tech Dev* Pte Ltd RUO-MKT-02-13399-A. 2021.
33. Khalaf K, Paoletti G, Puggioni F, et al. Asthma from immune pathogenesis to precision medicine. *Semin Immunol*. 2019;46:101294. doi:10.1016/j.smim.2019.101294
34. Gans MD, Gavrilova T. Understanding the immunology of asthma: pathophysiology, biomarkers, and treatments for asthma endotypes. *Paediatr Respir Rev*. 2020;36:118–127. doi:10.1016/j.prrv.2019.08.002
35. Tai W, Bhome AB, Tang P, Chan H-K, Kwok PCL. Indian generic fluticasone/salmeterol dry powder inhalers – an aerodynamic comparison. *Drug Deliv Lung*. 2020;31.
36. Demoly P, Hagedoorn P, de Boer AH, Frijlink HW. The clinical relevance of dry powder inhaler performance for drug delivery. *Resp Med*. 2014;108:1195–1203. doi:10.1016/j.rmed.2014.05.009
37. Hofmann W, Asgharian B, Bergmann R, Anjilvel S, Miller FJ. The effect of heterogeneity of lung structure on particle deposition in the rat lung. *Toxicol Sci*. 2000;53(2):430–437. doi:10.1093/toxsci/53.2.430
38. Shahin HI, Chablani L. A comprehensive overview of dry powder inhalers for pulmonary drug delivery: challenges, advances, optimization techniques, and applications. *J Drug Deliv Sci Technol*. 2023;84:104553. doi:10.1016/j.jddst.2023.104553